WARSAW UNIVERSITY OF TECHNOLOGY Index 351733
FACULTY OF CIVIL ENGINEERING
COMMITTEE FOR CIVIL AND WATER ENGINEERING
POLISH ACADEMY OF SCIENCES ISSN 1230-2945

DOI: 10.24425/ace.2026.1379

ARCHIVES OF CIVIL ENGINEERING

Vol. LXXII ISSUE 3 2026

pp. 213 – 225

Research paper

Experimental study of temperature field in cross section of concrete filled steel tube members

Qingchao Zhao[1], Qian Wei[2], Zongxian Gao[3], Zhengfei Liu[4], Lihe Mei[5]

Abstract: Experimental tests were conducted to investigate the temperature field within concrete filled steel tube(CFST). The study analyzed the circumferential and radial variations of the temperature field across the component's cross-section over time, under the influence of ambient temperature, solar radiation, and wind speed. The findings revealed notable nonlinearity in the temperature field concerning both time and cross-sectional position. Temperature peaks within the concrete varied in phase with respect to the central measurement point, indicating a discernible phase difference. Radially across the cross-section, temperature changes near the interior exhibited gradual variation, with minimal influence from external environmental factors. The temperature at the central point emerged as a product of various interacting factors, illustrating a degree of complexity. Drawing upon existing temperature gradient models, a temperature gradient formula incorporating multiple parameters such as solar radiation, ambient temperature, and wind speed was established through fitting procedures, and the accuracy of the fitted formula is good.

Keywords: concrete filled steel tube, nonlinear, section temperature field distribution, temperature gradient

[1]MSc., Shandong Hi-Speed Construction Management Group Co., LTD, Jinan, China, e-mail: 3988706413@qq.com, ORCID: 0009-0005-3533-3045
[2]MSc., Geotechnical and Structural Engineering Research Center of Shandong University, 17923 Jingshi Road, Jinan, China, e-mail: 493532127@qq.com, ORCID: 0009-0006-2400-8834
[3]MSc., Shandong Expressway Gaoshang Highway Co., LTD, Jinan, China, e-mail: 19863723610@163.com, ORCID: 0009-0003-0503-7363
[4]MSc., Shandong Expressway Gaoshang Highway Co., LTD, Jinan, China, e-mail: liuzhengfei7220@163.com, ORCID: 0009-0008-9790-4642
[5]MSc., Shandong Expressway Gaoshang Highway Co., LTD, Jinan, China, e-mail: meilihe8747@163.com, ORCID: 0009-0009-0645-8438

1. Introduction

Concrete filled steel tube (CFST) comprises a composite structure of steel and concrete. With concrete exhibiting a relatively low thermal conductivity, the temperature distribution within concrete filled steel tube structures demonstrates nonlinear characteristics under the influence of external environmental factors such as ambient temperature, solar radiation, wind speed, and inherent material properties. This results in significant deviations from the temperature distributions observed in singular concrete or steel structures . Therefore, it is imperative to conduct experimental and theoretical investigations into the temperature distribution of concrete filled steel tube structures under external environmental conditions. This endeavor aims to elucidate the internal temperature distribution of such structures and discern their patterns of variation. Certain scholars have conducted analyses on the variations in sectional temperature fields concerning the azimuth of sunlight exposure and the spatial distribution across the cross-section, based on temperature monitoring of concrete filled steel tube components [2–4]. Yang conducted a comparative experimental study on the temperature variations between concrete filled steel tube and plain concrete, utilizing outdoor environmental conditions and artificial climate simulations as research parameters. Hua obtained stress-strain curves for both concrete filled steel tube and plain concrete under temperature effects, and subsequently analyzed the debonding phenomenon in concrete filled steel tube. Zhou conducted full-scale temperature distribution monitoring experiments on concrete filled steel tube components. The findings indicate that in the winter conditions of the Qinghai-Tibet Plateau region, debonding at the ribs of concrete filled steel tube arches is highly prone to occurrence. Yan utilized a clear sky model and temperature field calculation theory to unveil the temperature distribution patterns across the transverse section of concrete filled steel tube arch ribs, along with their temporal variations. Yu through numerical simulations discovered that the solar temperature effect on arch ribs is significant under the most adverse solar temperature difference conditions. Liu [10, 11] monitored the structural temperature and meteorological parameters of CFST components with tilt angles of 0^{o}, 45^{o}, and 90^{o}, establishing an empirical formula for the maximum daily temperature difference of arbitrarily inclined concrete filled steel tube components. Ren based on three solar radiation models, simulated the impact of solar radiation on the temperature distribution of bridge structures. Yang conducted finite element analysis on the solar temperature field of large- diameter concrete filled steel tube components and proposed a temperature gradient model for the most unfavorable moments.

In summary, significant research achievements have been made regarding the temperature field distribution in concrete filled steel tube arch bridges. However, most literature exhibits relatively short testing periods and limited consideration of the effects of atmospheric radiation, wind speed, and atmospheric temperature on sectional temperature fields. This study focuses on concrete filled steel tube components and conducts experimental tests on sectional temperature fields to investigate the distribution patterns under solar radiation and atmospheric temperature.

Additionally, based on existing temperature gradient models, a temperature gradient formula incorporating multiple parameters such as solar radiation, atmospheric temperature, and wind speed has been established.

2. Temperature field test of concrete filled steel tube section

2.1. Specimen size and measurement point arrangement

The specimen dimensions are as follows: length of 1 meter, diameter of 0.93 meters, and wall thickness of 35 mm. A test section is arranged along the longitudinal mid-span section. Along the radial direction of the test section, measurement points are placed at intervals of $D/6$, totaling 50 measurement points, as shown in Fig. 1.

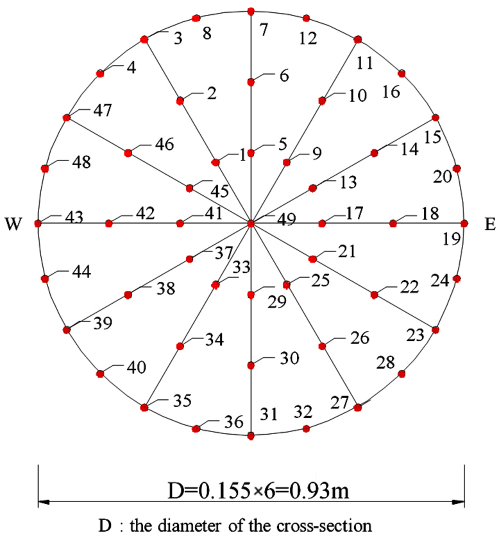

Fig. 1. Schematic of measurement points

2.2. Data acquisition system and steel pipe preparation

The temperature and solar radiation testing utilized the pre-embedded JMT-36C intelligent temperature sensor and JMGD-1G solar radiation sensor. Data collection was facilitated by a wireless remote automation acquisition module, with a sampling frequency of 1 reading every 20 minutes. The testing equipment is depicted in Fig. 2, and the on-site arrangement is illustrated in Fig. 3, a round hole with a diameter of 20 cm is made on the wall of the steel pipe before pouring, and the hole is sealed after the concrete pouring is completed.

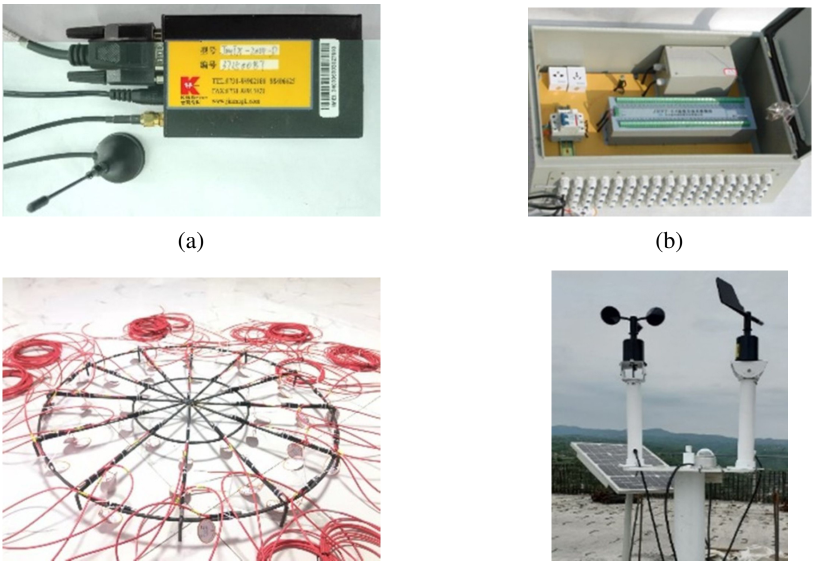

(a) (b)

(c) (d)

Fig. 2. Schematic diagram of test equipment; (a) DTU, (b) Integrated Acquisition Module, (c) Sensor arrangement, (d) Wind speed and solar radiation sensors

Fig. 3. Test Site Setup

3. Analysis of test results

The temperature detection period for the concrete filled steel tube component spanned from January 31st, 2021, to November 18th, 2021. Unfortunately, due to equipment malfunctions during the testing period, the collected data was lost. However, leveraging the existing data should suffice for studying the variation patterns of the sectional temperature field.

3.1. Atmospheric temperature

Daily maximum temperature, minimum temperature, and maximum atmospheric temperature difference are depicted in Fig. 4.

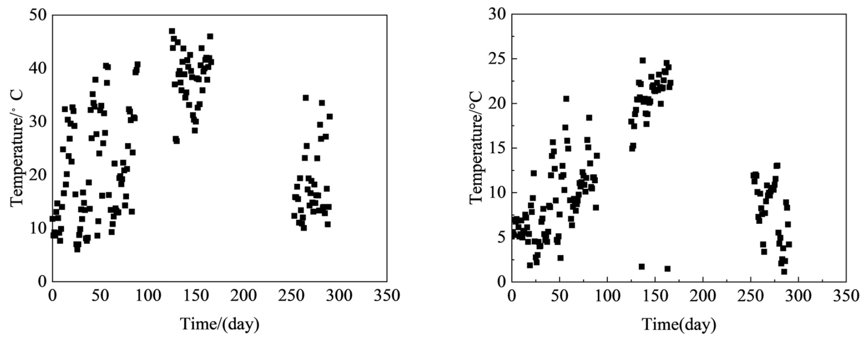

(a) (b)

Fig. 4. Daily atmospheric temperature records during the test period; (a) Daily maximum temperature, (b) Daily minimum temperature

Based on Fig. 4, it is evident that the highest recorded atmospheric temperature occurred on June 6th, reaching 46.99°C. The lowest temperature was observed on November 12th, with a reading of 1.17°C. Additionally, the daily maximum atmospheric temperature difference reached as high as 31.45°C.

3.2. Law of change of cross-section temperature in circumferential and radial directions

3.2.1. Temperature distribution pattern of measuring points along the cross-section ring direction

Figure 5 displays the daily temperature variation curves for interface measurement points 15 and 47, central measurement point 49, and atmospheric temperature measurement point 50. Additionally, temperature curves for internal concrete measurement points 2, 6, 10, 14, and 46, as well as 1, 5, 9, 13, and 45, are plotted separately, as depicted in Fig. 5– 7, it can be observed that:

1. The temperature variations at each measurement point exhibit periodicity, displaying both maximum and minimum temperature values over the entire cycle, indicative of a harmonic periodic pattern.
2. Measurement points 15 and 47 are significantly influenced by solar radiation, resulting in distinct differences in temperature curves. At measurement point 15, the morning solar radiation peaks at 13:20, while at measurement point 47, the afternoon solar radiation peaks at 5:20 PM. The peak atmospheric temperature (measurement point 50) occurs at 3:00 PM.
3. The temperature fluctuation range is the largest at $D/2$ from the center of the steel pipe, and the smallest at $3/D$. The closer you get to the center, the smaller the range.

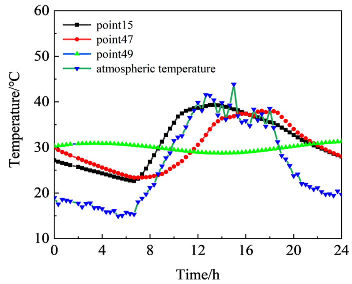

Fig. 5. Daily temperature curve at the position $D/2$ from the center of the section

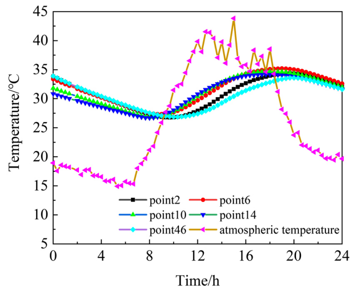

Fig. 6. Daily temperature curve at the position $2D/3$ from the center of the section

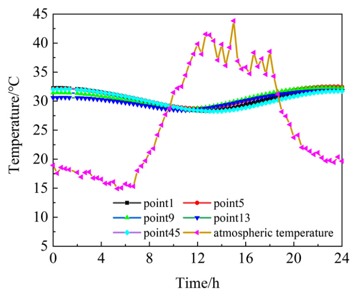

Fig. 7. Daily temperature curve at the position $D/3$ from the center of the section

3.2.2. Temperature distribution pattern of measurement points along the radial direction of the cross-section

Analyzing the temperature distribution along the radial direction of the section at measurement points 13, 14, 15, and 49, as shown in Fig. 8, the following observations can be made:

1. Measurement point 15, under the combined influence of solar radiation and atmospheric temperature, initially reaches its temperature peak. The temperature rise at points 14 and 13 is slower, with peaks occurring at 18:20 and 23:00, respectively. This indicates a lag in the temperature rise of internal concrete, with peaks occurring later as the concrete approaches the center.

2. After 18:00, solar radiation and atmospheric temperature weaken, leading to a decrease in temperature at measurement point 15. Due to concrete's higher specific heat capacity compared to the steel pipe, the temperatures at points 14 and 13 continue to rise. At this point, the temperature distribution across the section exhibits a pattern of outer lower and inner higher temperatures.
3. There are differences in the times at which temperature peaks occur along the radial direction. Closer proximity to the center results in smoother temperature variation curves, with less influence from atmospheric temperature, solar radiation, and wind speed.

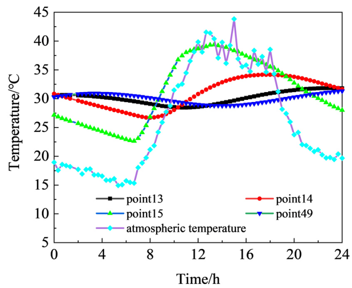

Fig. 8. Daily temperature profiles of radial measurement points

3.3. Law of change of cross-section temperature with time

Based on the temperature monitoring data from measurement points 1 to 49, a contour plot of isotherms at a typical moment is depicted in Fig. 9, the following insights can be gleaned:

1. At 5:20 AM, the atmospheric temperature reaches its lowest point (14.93°C). Compared to daytime, temperature fluctuations are minimal during the night, resulting in a nearly uniform temperature distribution across the section.
2. Following sunrise, the sectional temperature field transitions to a non- uniform state due to the effects of solar radiation and atmospheric temperature. While temperatures rise overall, the central point continues to experience cooling. At 12:40 PM, the temperature reaches its lowest point (28.35°C). During this time, the sectional temperature field exhibits its most pronounced nonlinearity of the day, with almost no closed isotherms across the section.
3. At 3:00 PM, the atmospheric temperature reaches its maximum value (43.84°C). As the temperature at the center point of the section rises, closed isotherms begin to form in the sectional temperature field, albeit with the center of the temperature field skewed towards the lower section of the profile. Subsequently, as the western side is exposed to sunlight, by 5:20 PM, the temperature at measurement point 47 on the west side reaches its maximum value (38.03°C).
4. With the decrease in atmospheric temperature and the weakening of solar radiation, the exterior surface of the steel pipe and the outer edge of the concrete begin to cool down. However, due to the lag in temperature changes at the central point, it continues to receive heat transfer from other points, resulting in a continued rise in temperature.

At 2:00 AM the following day, the temperature reaches its maximum value (32.25°C). At this point, the sectional temperature field exhibits a pattern of outer lower and inner higher temperatures. Subsequently, the overall temperature continues to decline and tends towards a uniform distribution.

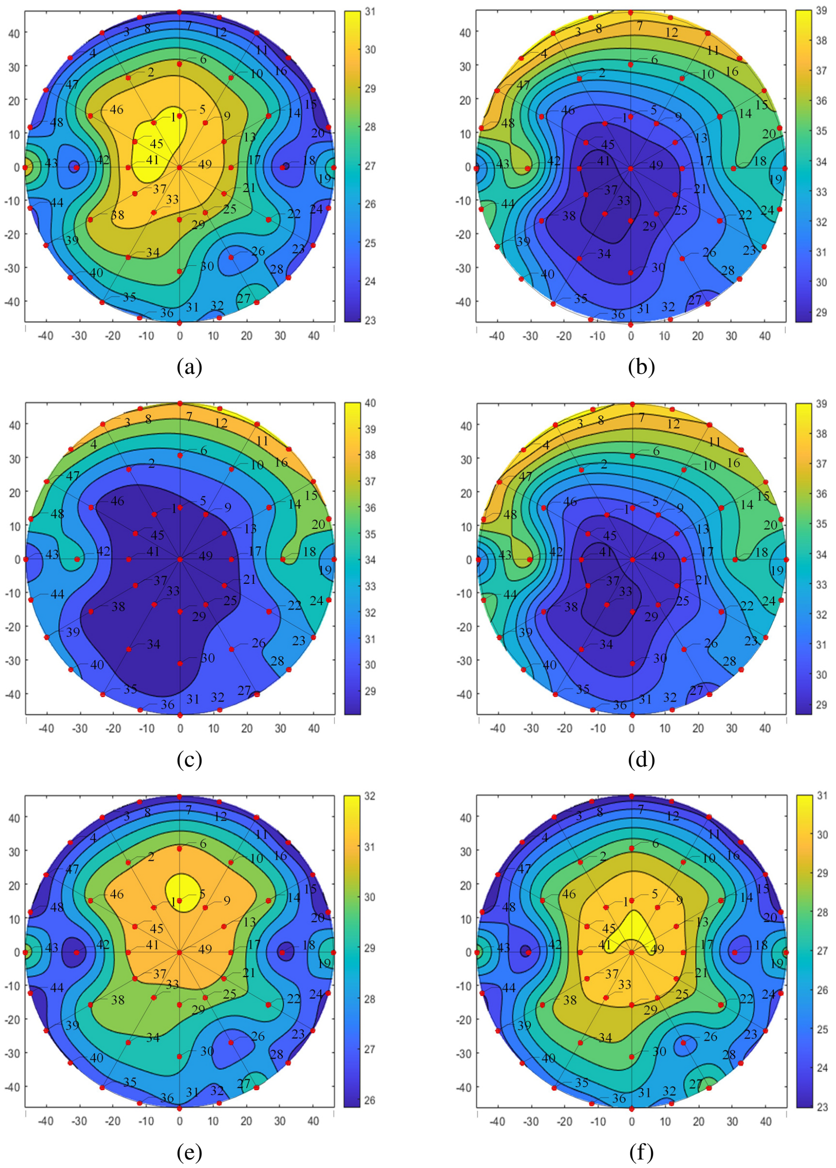

Fig. 9. Isotherm cloud map of cross-section at typical moments; (a) (5:20), (b) (12:40), (c) (15:00), (d) (17:20), (e) 2:00 the next day, (f) 5:40 the next day

3.4. Cross-sectional temperature gradient

Literature [10] established a calculation formula for the sectional temperature gradient, with a schematic diagram depicted in Fig. 10.

$$T^+(y) = \begin{cases} T_1^+\left(\frac{Dt^+ - y}{Dt^+}\right)^{n_1^+} & 0 \le y \le D_t^+ \\ T_2^+\left(\frac{y - D_t^+}{D - D_t^+}\right)^{n_2^+} & D_t^+ < y \le D \end{cases} \tag{3.1}$$

$$T^-(y) = \begin{cases} T_1^-\left(\frac{Dt^- - y}{Dt^-}\right)^{n_1^-} & 0 \le y \le D_t^- \\ T_2^-\left(\frac{y - D_t^-}{D - D_t^+}\right)^{n_2^-} & D_t^- < y \le D \end{cases} \tag{3.2}$$

where: $T^+(y)$ – the positive temperature gradient (°C), $T^-(y)$ – the negative temperature gradient (°C), T_1^+ – the maximum positive temperature gradient on the sunny side, T_2^+ – the maximum positive temperature gradient on the shaded side, D_t^+ – the range of distribution of T_2^+, D – the diameter of the cross-section, T_1^- – the maximum negative temperature gradient on the sunny side, T_2^- – the maximum negative temperature gradient on the shaded side, D_t^- – the distribution range of T_2^-, $n_1^+, n_2^+, n_1^-, n_2^-$ – the coefficients to be determined.

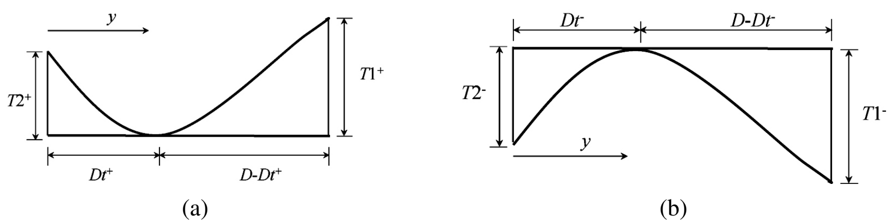

Fig. 10. Temperature gradient diagram; (a) Schematic of the forward temperature gradient, (b) Negative Temperature Gradient Schematic

The maximum temperature gradient data of measuring points 7 and 31 (Table 1) were brought into the temperature gradient calculation formula for fitting, and the fitting values of each coefficient were obtained (Table 2). The fitting effect was good, and the distribution diagram of the most unfavorable temperature gradient in the cross-section was drawn accordingly, as shown in Fig. 11.

Table 1. Maximum temperature gradient

Measurement point location	Positive temperature gradients		Negative temperature gradients	
	Dates	Maximum temperature gradient (°C)	Dates	Maximum temperature gradient (°C)
Measurement point 7	2021-4-29 16:20	19.44	2021-2-2 6:00	–17.05
Measurement point 31	2021-3-24 17:40	5.28	2021-2-2 7:00	–15.74

Table 2. Maximum temperature gradient fitting parameters

	Positive temperature gradients						Negative temperature gradients						
D_t^+	T_1^+	n_1^+	R^2	T_2^+	n_2^+	R^2	D_t^-	T_1^-	n_1^-	$R2$	T_2^-	n_2^-	R^2
$D/3$	19.44	2.97	0.9988	5.28	1.60	1	$D/2$	–17.05	2.39	0.9997	–15.74	1.78	0.9995

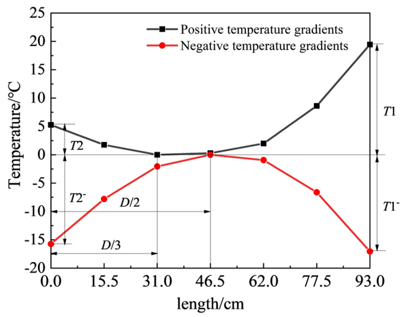

Fig. 11. Distribution of the most unfavourable temperature gradient in the cross section

For concrete filled steel tube components, there is a scarcity of sectional temperature gradient formulas that consider multiple parameters. Lee [14] and Pottieter [15] have established temperature gradient prediction formulas specifically for concrete box girder sections, leading to the determination of the following fitting formula format:

$$T = \left(AI^2 + BI\right) + CN + \left(Dv^3 + Ev^2 + Fv\right) + G \tag{3.3}$$

where: A, B – coefficients characterising the effect of solar radiation, C – the coefficient characterising the effect by the atmosphere, D, E, F – coefficients characterising the effect of wind speed, G – the coefficient characterising the temperature residuals, I – the total daily solar radiation (MJ/m^2), N – the daily atmospheric temperature change (°C), v – the daily mean wind speed (m/s), T – the temperature gradient.

Based on the test data, the coefficients of determination for the fitted formulas are presented in Table 3, and the fitting formula calculation results compared with the measured values, as shown in Figure. 12, the fitting effect was good.

Table 3. Equation coefficient to be determined

Parameters	$T1$	$T2$
A	–0.01202	–0.001325
B	0.8313	0.1052
C	0.1557	0.06795
D	1.4833	0.5003
E	–2.0213	–1.3695
F	–0.2001	1.0858
G	–1.8479	0.09086
$R2$	0.921	0.701

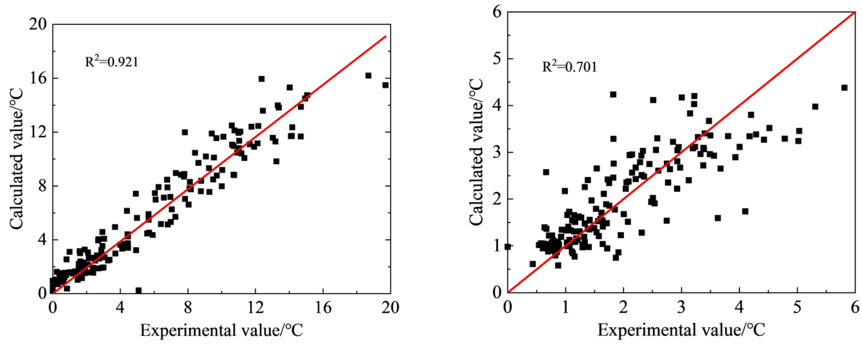

(a) (b)

Fig. 12. Comparison of measured and predicted values; (a) $T1$, (b) $T2$

The measured frequencies of Atmospheric temperature, Wind speed and Solar radiation in the measured data were counted to obtain the external environment frequency histogram, and the lognormal distribution was processed to obtain the environmental characteristic values, as shown in Table 4.

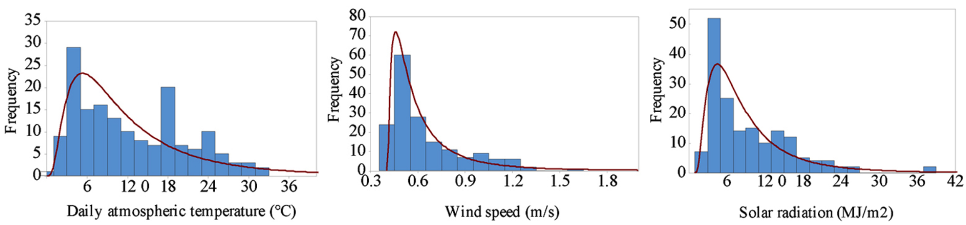

(a) (b) (c)

Fig. 13. Frequency histogram of the external environment; (a) Daily atmospheric temperature, (b) Average wind speed, (c) solar radiation

Table 4. Statistics on environmental eigenvalues

Parameter	Distributional characteristics	Position parameter	Scale parameter	Thresholds	Eigenvalue type	Eigenvalue
Atmospheric temperature	log-normal	2.560	0.5956	–2.316	98% guarantee ceiling	39.36
Wind speed	log-normal	–1.868	1.026	0.4016	98% guarantee ceiling	1.672
Solar radiation	log-normal	1.858	0.763	0.896	98% guarantee ceiling	31.62

By substituting the environmental characteristic values into Formula 3, we obtain T_1 = 19.496°C and T_2 = 5.092°C. Meanwhile, based on the calculations from literature [10], we obtain T_1 = 19.44°C and T_2 = 5.28°C. The small difference between the two sets of values indicates that the multiple-parameter fitting formula considering external environmental factors predicts the sectional temperature gradient effectively.

4. Conclusions

The experiment conducted on the sectional temperature field of concrete filled steel tube components, coupled with the analysis of temperature sensor, atmospheric radiation sensor, and wind speed and direction sensor data, has revealed the following conclusions:

1. There exists a phase difference between the temperature peaks of internal concrete measurement points and the central measurement point. The temperature at the central point demonstrates a certain level of complexity, representing the combined effects of various factors.
2. Along the radial direction of the section, the temperature variation of internal measurement points is relatively gradual, with minimal influence from external environmental factors such as solar radiation, atmospheric temperature, and wind speed.
3. Based on the existing temperature gradient model, a temperature gradient formula considering multiple parameters including solar radiation, atmospheric temperature, and wind speed has been established.

References

[1] Y.J. Liu, J. Liu, and N. Zhang, "A review of research on sunlight temperature effects on bridge structures", *Journal of Civil Engineering*, vol. 52, no. 5, pp. 59–78, 2019.

[2] T. Zhou, H.J. Yang, J.J. Hu, H.N. Liu, H.B. Liu, and Z.H. Chen, "Measured temperature field of rectangular steel tubular concrete members section under exposed environment", *Building Structures*, vol. 50, no. 7, pp. 80–85, 2020, doi: 10.19701/j.jzjg.2020.07.012.

[3] Y. He, M. Ding, Q. Zhang, and H.C. Zheng, "Experimental study on the temperature field of steel pipe concrete members under sunlight", *Journal of Qingdao University of Science and Technology*, vol. 33, no. 3, pp. 307–311, 2012, doi: 10.16351/j.1672-6987.2012.03.005.

[4] B.C. Chen and Z.Y. Liu, "Measured analysis of temperature field of steel pipe concrete members under sunlight", *Highway Traffic Science and Technology*, pp. 117–122, 2008.

[5] Y. Yang, R.L. Zhang, Q. Qi, and H.P. Yang, "Experimental study on temperature field distribution of large diameter circular steel pipe concrete section", *Building Structure*, vol. 50, no. 17, pp. 99–103, 2020, doi: 10.19701/j.jzjg.2020.17.016.

[6] D.Q. Hua, "Analysis of temperature field of steel pipe concrete in arch bridge", *Railway Construction*, vol. 5, pp. 13–15, 2017.

[7] D.W. Zhou, N.C. Deng, X. Guo, and T. Shi, "Temperature effect of large temperature difference in steel-tube concrete arch bridge in Qinghai-Tibet Plateau region", *Journal of Guilin University of Technology*, vol. 40, no. 4, pp. 735–741, 2020.

[8] R.Z. Yan, J.Q. Liu, and S.L. Liu, "Analytical and experimental study on inhomogeneous temperature field of steel-tube concrete arch and its de- embedding caused by solar radiation", *Chinese Journal of Highways*, vol. 34, no. 1, pp. 79–92, 2021, doi: 10.19721/j.cnki.1001-7372.2021.01.008.

[9] M.S. Yu, N. Deng, L. Wang, and Z. Zhang, "Study on the temperature effect of sunshine on steel-tube concrete arch ribs of mega arch bridges", *Highway Engineering*, vol. 46, no. 3, pp. 99–104, 2021, doi: 10.19782/j.cnki.1674-0610.2021.03.015.

[10] J. Liu, Y. Liu, G. Zhang, L. Jiang, and X. Yan, "Prediction Formula for Temperature Gradient of Concrete-Filled Steel Tubular Member with an Arbitrary Inclination", *Journal of Bridge Engineering*, vol. 25, no. 10, art. no. 04020076, 2020, doi: 10.1061/(ASCE)BE.1943-5592.0001599.

[11] J. Liu, Y. Liu, and G. Zhang, "Experimental Analysis of Temperature Gradient Patterns of Concrete-Filled Steel Tubular Members", *Journal of Bridge Engineering*, vol. 24, no. 11, art. no. 04019109, 2019, doi: 10.1061/(ASCE)BE.1943-5592.0001488.

[12] Z. Ren, S. Hu, and Q. Ding, “Study on the effect of solar radiation modelling on the temperature field of steel pipe concrete piers”, *Engineering Mechanics*, vol. 27, no. 4, pp. 246–250+256, 2010.

[13] D. Yang, G. Chen, X. Ding, and J. Xu, “Thermal field of large diameter concrete filled steel tubular members under solar radiation”, *Computers and Concrete*, vol. 26, no. 4, pp. 343–350, 2020.

[14] J. Lee and I. Kalkan, “Analysis of thermal environmental effects on precast, prestressed concrete bridge girders: temperature differentials and thermal deformations”, *Advances in Structural Engineering*, vol. 15, no. 3, pp. 447–459, 2012, doi: 10.1260/1369-4332.15.3.447.

[15] S.R. Abid, N. Tayşi, and M. Özakça, “Experimental analysis of temperature gradients in concrete box-girders”, *Construction and Building Materials*, vol. 106, pp. 523–532, 2016, doi: 10.1016/j.conbuildmat.2015.12.144.

Received: 2024-06-15, Revised: 2024-11-03